

Theoretical Investigations on the Conformation of the β -D-Arabinofuranoside Ring

Hashem A. Taha,[†] Pierre-Nicholas Roy,[‡] and Todd L. Lowary^{*,†}

Department of Chemistry and Alberta Ingenuity Centre for Carbohydrate Science, Gunning-Lemieux Chemistry Centre, University of Alberta, Edmonton, AB, Canada T6G 2G2 and Department of Chemistry, University of Waterloo, Waterloo, ON, Canada N2L 3G1

Received August 12, 2010

Abstract: A method for the conformational analysis of furanose rings that involves the prediction of $^3J_{\text{H,H}}$ that can be compared directly to experimental values is investigated. This method, which differs from the traditional PSEUROT approach for conformational studies of furanose rings, was previously applied to a number of α -D-arabinofuranosides and enabled the direct comparison of $^3J_{\text{H,H}}$ values to those obtained from NMR spectroscopy. In this paper, the use of this approach to study the conformational preferences of oligosaccharides containing β -linked arabinofuranose residues is reported. Density functional theory (DFT) calculations were carried out to derive Karplus relationships that are specifically tailored for these ring systems. In addition, probability distributions obtained from GLYCAM/AMBER molecular dynamics simulations were employed to calculate $^3J_{\text{H,H}}$ values from these Karplus relationships. However, unlike the results obtained with α -arabinofuranosides, the $^3J_{\text{H,H}}$ values computed for β -arabinofuranosides agreed poorly with experimental values. This prompted the exploration of other methodologies including reevaluation and optimization of the initial MD protocol, use of various force field models, and recalculation of the DFT-derived coupling profiles using an optimized basis set. After extensive investigations, we established that the conformer distributions obtained from MD simulations with the GLYCAM force fields and the furanoside-specific CHARMM force field in combination with the DFT Karplus equations, determined using an augmented basis set (B3LYP/aug-cc-pVTZ-J), produced the best agreement compared to experimental $^3J_{\text{H,H}}$ values. Using these protocols, there is relatively good agreement in $^3J_{\text{H,H}}$ for all coupling pathways with the exception of $^3J_{2,3}$ and $^3J_{3,4}$, which are underestimated.

Introduction

Furanose (or five-membered ring) carbohydrates are important constituents of a number of glycoconjugates in many microorganisms.^{1–4} Our group has a long-standing interest in conformational analysis of furanoside-containing polysaccharides found in the complex cell wall of the pathogenic species *Mycobacterium tuberculosis*, the causative agent of tuberculosis.^{5–8} Due to the critical role that these glycoconjugates play in the viability and virulence of mycobacteria,⁹

it is essential to study their conformation in order to understand their biological functions.

Furanose rings assume various twist (T) and envelope (E) conformations that can be depicted using the pseudorotational wheel (Figure 1). Each conformer is described by its Altona–Sundaralingam (AS) phase angle of pseudorotation (P), which represents the atoms that are displaced from the plane, and its AS puckering amplitude (ϕ_m), a measure of the maximum displacement from the planar ring form. Given five endocyclic torsion angles of a particular conformer, P and ϕ_m can be calculated.¹⁰ These conformers interconvert readily because of the relatively low-energy barriers separat-

* Corresponding author. E-mail: tlowary@ualberta.ca.

[†] University of Alberta, Edmonton.

[‡] University of Waterloo.

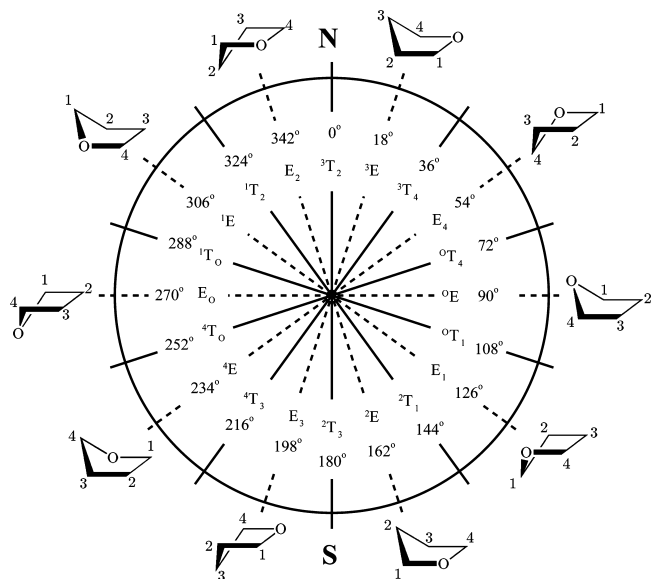


Figure 1. Pseudorotational itinerary for a D-furanose ring.

ing them ($<5 \text{ kcal mol}^{-1}$).¹¹ This ring flexibility poses a challenge for the theoretical description of furanosides as both ring torsion angles as well as any exocyclic dihedral angles must be considered.

NMR spectroscopy has played a key role in the determination of the solution conformation of carbohydrates.^{12–14} In particular, for furanosides, three-bond hydrogen–hydrogen coupling constants ($^3J_{\text{H,H}}$) obtained from NMR spectroscopy are commonly used in conjunction with a computer program, PSEUROT, to predict their conformational preferences.^{10,15–18}

This program assumes an equilibrium between two low-energy conformers, often located in the northern and southern hemispheres of the pseudorotational wheel, which interconvert through pseudorotation (Figure 1). This program takes experimental $^3J_{\text{H,H}}$ values for the ring hydrogens and calculates, using the appropriate Karplus relationships, two conformations and their mole fractions that fit the data the best. Although PSEUROT has been commonly employed for conformational analysis of five-membered rings, there are drawbacks to its use. For example, the two-state model is not valid in all cases, and the analysis may sometimes provide physically unrealistic conformations.^{8,19,20} As an alternative, we have used theoretical models, such as molecular dynamics (MD) simulations together with density functional theory (DFT) calculations, to study conformation and dynamics.^{6–8}

In a previous investigation,⁸ we reported MD simulations of a number of oligosaccharides containing α -arabinofuranose (α -Araf) residues. β -Arabinofuranose (β -Araf) moieties are also found in nature, and these glycosidic residues play important roles within the cell wall structure of *M. tuberculosis*. In fact, β -Araf residues (e.g., **1–5**, Figure 2) are usually found at the periphery of mycobacterial cell wall polysaccharides and are typically substituted with other groups that play key roles in the survival and pathogenicity of the organism.¹ In the arabinogalactan (AG), this group is esterified with mycolic acids,¹ while in the lipoarabinomannan (LAM), this position is capped by short mannapyranosyl oligosaccharides that are important in interactions with human mannose binding receptors.^{21–23} One of our interests

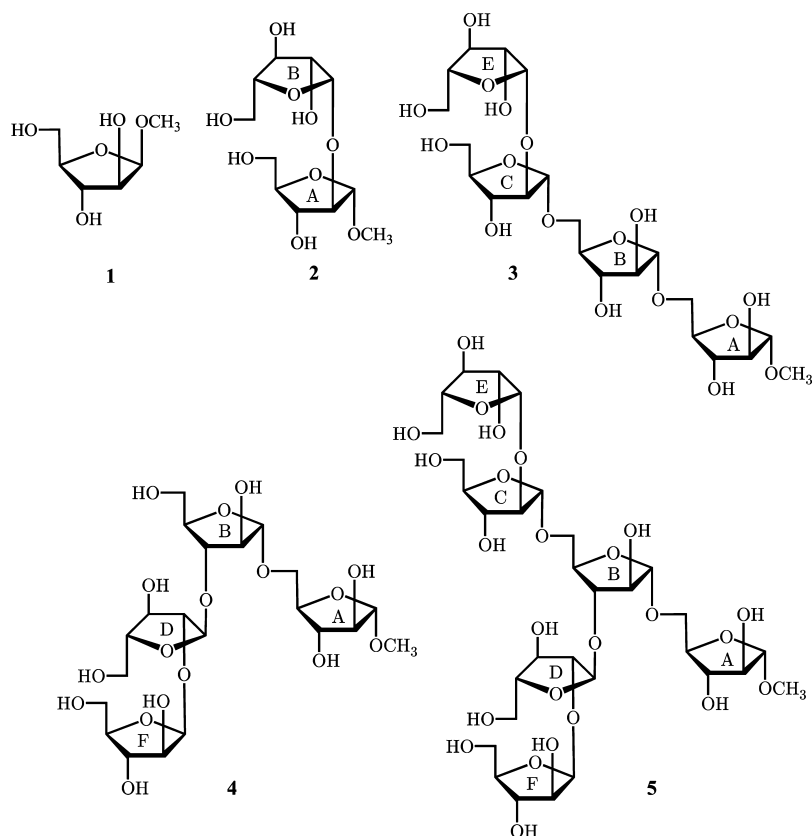


Figure 2. Studied β -Araf-containing molecules.

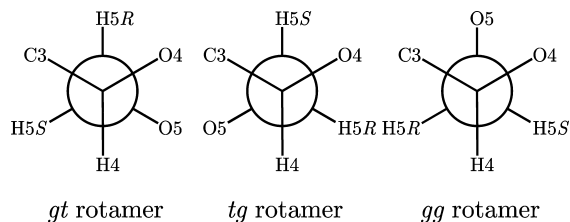


Figure 3. Definition of staggered rotamers about the C4–C5 bond.

is a hexasaccharide motif found at the nonreducing end of AG and LAM that is comprised of both α - and β -Araf residues (**5**, Figure 2). It has been suggested that this hexasaccharide plays an important role in a number of immunological events that occur upon infection by mycobacteria.^{24,25} For example, we have demonstrated that this motif is recognized by the anti-LAM antibody CS-35,^{26,27} and thus this structure elicits an immune response.

Previously, we reported the use of the AMBER/GLYCAM approach to study the conformation of methyl β -D-arabinofuranoside (**1**, Figure 2), and in the course of these studies we demonstrated that the water model used had an important influence on the ability of this method to reproduce experimentally determined conformer populations.⁷ More recently, we reported an alternative method to study the conformational preferences of α -Araf systems.⁸ This protocol involves the use of probability distributions from MD simulations to calculate Boltzmann-averaged $^3J_{\text{H,H}}$ values in combination with DFT-derived Karplus equations. The resulting coupling constants can be directly compared to those obtained from NMR spectroscopy. Better agreement with experiment was found using the DFT-derived Karplus equations compared to the use of the empirical Haasnoot–Altona Karplus relationship.²⁸ This approach provided an alternative to the use of PSEUROT for studying furanose conformation; notably, it does not require the two-state assumption.

In concert with MD simulations performed on oligosaccharides containing α -Araf residues,⁸ the use of the AMBER/GLYCAM approach is employed here to study the conformation of oligofuranosides containing β -Araf residues (**1–5**, Figure 2). Although the use of this method was successful in probing the conformation of α -Araf glycosides, its use in probing β -Araf conformation proved problematic. In the present report, we investigate the potential sources of these problems, and a discussion of the various methods employed toward finding solutions is included.

Nomenclature

The three ideally staggered rotamers about the C4–C5 bond (gt, tg, and gg) in the Araf residues are defined as shown in Figure 3.

Methods

DFT $^3J_{\text{H,H}}$ Coupling Profiles. In a manner similar to previously reported for methyl α -D-arabinofuranoside,⁸ 10 envelope conformers of methyl β -D-arabinofuranoside (**1**) corresponding to all envelope structures indicated on the pseudorotational wheel (Figure 1) were constructed. For each

envelope structure, three C4–C5 rotamers (gt, tg, gg) and three C5–O5 rotamers ($\psi = 180^\circ$, -60° , and 60° , where ψ is defined by the H5–O5–C5–C4 torsion angle) were generated, resulting in a total of 90 conformations. The geometries of all 90 conformations were then optimized with Gaussian 03²⁹ using the B3LYP functional³⁰ with the 6-31G* basis set. The torsion angle representing the four-atom plane of each envelope conformer was fixed at 0° to maintain the envelope structure. For example, the E_0 conformer was generated by fixing C1–C4 in the plane. All other geometric parameters were allowed to vary during the geometry optimizations.

DFT calculations of the spin–spin coupling constants in **1** were initially performed using Gaussian 03²⁹ at the B3LYP/cc-pVTZ level of theory.^{30,31} All four contributions to the $^3J_{\text{H,H}}$ were computed (Fermi contact, diamagnetic spin orbit, paramagnetic spin orbit, and spin dipolar). The resulting J data were extracted for all conformations (see Table S-1 in the Supporting Information for complete coupling constant data).

The same spin–spin coupling calculations were also performed with an augmented basis set (aug-cc-pVTZ-J) that contains additional primitive s and p functions (compared to cc-pVTZ) and has been optimized for calculation of spin–spin coupling constants.^{32–34} For comparison, a basis set [5s2p1d3s1p] developed in the Serianni and Carmichael groups, designed to recover the Fermi contact contribution to the coupling,³⁵ was also employed. This basis set has been shown to provide good agreement with experimental $^3J_{\text{H,H}}$.³⁵ In addition, calculations with this basis set were much faster compared to the aug-cc-pVTZ-J calculations.

The Marquardt–Levenberg nonlinear least-squares algorithm³⁶ was used to fit the acquired coupling constants to the following truncated Fourier series in the H,H dihedral angle, ϕ :³⁷

$$^3J_{\text{H,H}} = a + b \cos(\phi) + c \cos(2\phi) \quad (1)$$

The coefficients a – c are obtained, corresponding to the five $^3J_{\text{H,H}}$ coupling pathways in **1**. In the particular cases of $^3J_{1,2}$, $^3J_{2,3}$, and $^3J_{4,5\text{R}}$, a phase shift to the dihedral angle (ϕ) was required to obtain improved fits.

GLYCAM04 MD Simulations. Initial simulations of **1** were carried out using the PMEMD implementation in the AMBER 10 suite of programs³⁸ with the AMBER force field and the GLYCAM carbohydrate parameter set (version 04f).³⁹ A four-step equilibration scheme was performed on **1** with an initial minimization step where the sugar was held fixed and the positions of water molecules were relaxed. A subsequent minimization allowed for all atoms to move for 50 steps of steepest descent followed by 950 steps of conjugate gradient to minimize the system as a whole.

Once sufficiently relaxed, the system underwent 100 ps of simulated annealing. The volume was kept constant, and the SHAKE⁴⁰ algorithm was used to constrain bonds involving hydrogen atoms. The final step before production dynamics involved equilibration of the physical parameters, such as temperature, pressure, and density of the system. This equilibration period was run over 240 ps using NPT

conditions, where temperature and pressure were held constant using a constant temperature thermostat with the weak coupling algorithm ($ntt = 1$)⁴¹ and a constant pressure barostat with isotropic position scaling ($ntp = 1$), respectively.

The production phase was run for 250 ns under identical NPT conditions as the final equilibration step. This longer simulation time was chosen to ensure sufficient equilibration of the system and proper convergence. SHAKE was used, and long-range electrostatic interactions were calculated using the particle mesh Ewald (PME) algorithm^{42,43} with a cutoff of 8 Å. Coordinates were printed to the trajectory file every 1000 steps (every 2 ps).

GLYCAM06 MD Simulations. MD simulations of **1–5** were also performed using the GLYCAM06 force field⁴⁴ and the AMBER 10 suite of programs.³⁸ Oligosaccharides **2–5** were constructed from multiple units of the α and β anomers of **1** using additive atomic charges as described previously.⁸ All other procedures are identical to the GLYCAM04 simulations.

Langevin Thermostat Simulations. MD simulations of **1** were carried out using a Langevin dynamics temperature regulation scheme⁴⁵ ($ntt = 3$) with a collision frequency (γ) of 2.0 ps^{-1} to address the validity of the algorithm used for maintaining a constant temperature throughout the simulations. Other simulation parameters remained unchanged.

Biased MD Simulations. A biased set of 200 conformations having P values in the range of $P = -5^\circ$ to 30° was generated from a 50 ns MD simulation. Partial atomic charges for these conformers were calculated as previously reported;^{6,7} the procedure and the resulting charges are included in the Supporting Information (Table S-2 and related discussion). Using this biased set of charges, MD simulations of **1** were carried out as before with no changes to the parameters indicated above.

CHARMM MD Simulations. MD simulations of **1** were also performed with the CHARMM program⁴⁶ in the constant pressure-constant temperature (NPT) ensemble using a Nosé–Hoover thermostat^{47,48} with a reference temperature of 300 K and a Langevin piston barostat⁴⁹ with a reference pressure of 1 atm. The system was built using the force field parameters reported by Hatcher et al. for aldopentofuranosides⁵⁰ and was solvated via the CHARMMing web interface⁵¹ with a cubic solvation of TIP3P water⁵² molecules with a crystal dimension of 17.57 Å. The system then underwent 50 steps of steepest descent and 950 steps of conjugate gradient minimization, which was followed by a 100 ps period of gradual heating to a final temperature of 300 K. The system was equilibrated for 240 ps under NPT conditions. The production dynamics were run for 250 ns at 300 K, and the SHAKE algorithm was used to constrain all hydrogen atom bonds to their equilibrium length and to maintain rigid TIP3P water geometry. The long-range electrostatic interactions were treated with the PME summation.

QM/MM Simulations. Hybrid quantum mechanical and molecular mechanical (QM/MM) simulations of **1** were performed in a cubic box of 264 TIP3P water molecules⁵² using the SANDER module in the AMBER 10 suite of programs.³⁸ The carbohydrate was treated using the semiempirical PM3CARB-1 parameter set,⁵³ and the solvent mol-

ecules were modeled classically. The PM3CARB-1 QM level of theory has been shown⁵³ to provide improved predictions for intramolecular hydrogen bonds, which are essential for correctly describing carbohydrates in an aqueous environment. Moreover, this level of theory was shown to improve predictions of structure and energetics of small carbohydrate analogues when compared to PM3.^{53,54} In our simulations, there are no bonds that cross the QM/MM boundary, and therefore, hydrogen link atoms were not required (i.e., there are no covalent bonds between QM and MM atoms). Preparation of the system for production dynamics included a 1000 step minimization, followed by a 100 ps simulated annealing period and a 240 ps equilibration. All steps were run using QM/MM. The SHAKE algorithm was used to constrain all hydrogen atom bonds, and long-range electrostatics were treated with the PME algorithm using a cutoff of 8 Å. Coordinates were printed to the trajectory file every 500 steps (every 1 ps).

GROMACS MD Simulations. MD simulations of **1** were also performed using the GROMACS program⁵⁵ together with the GROMOS96 force field⁵⁶ and the SPC/E water model.⁵⁷ Partial atomic charges calculated using our modified GLYCAM approach (as described previously)^{6,7} were used. The simulated system was composed of one molecule of **1** surrounded by 431 water molecules in a cubic box simulated under periodic boundary conditions. Newton's equations of motion were integrated using the GROMACS MD integrator with a 2 fs time step. The LINCS algorithm⁵⁸ was applied to constrain all bond lengths. The simulations were carried out in the NPT ensemble (at a constant temperature of 300 K and a pressure of 1 atm). The temperature and pressure were maintained constant using the weak-coupling Berendsen thermostat⁴¹ and the Berendsen barostat via isotropic coordinate scaling.⁴¹ The PME algorithm was used for treatment of electrostatics with a cutoff of 8 Å. Prior to production, the system was subjected to the three-step protocol (minimization, annealing, and equilibration) used in the other simulations. MD simulations were then conducted in the NPT ensemble for 200 ns, and data were collected every 2 ps.

$^3J_{\text{H,H}}$ from MD Conformer Ensembles. For an accurate comparison of the DFT/MD-derived $^3J_{\text{H,H}}$ values to experiment, ensemble averaging must be carried out. This was done by calculating $^3J_{\text{H,H}}$ values for each relevant fragment in compounds **1–5** using DFT-determined Karplus equations ($J(\phi)$, eq 2) in combination with the continuous probability distributions ($\rho(\phi)$, eq 2) of the respective $\phi_{\text{H,H}}$ obtained from MD simulations. In a similar manner as before,⁸ these $^3J_{\text{H,H}}$ values were then ensemble-averaged using the following relation:

$$\langle J \rangle = \int_0^{360} J(\phi) \rho(\phi) d\phi \quad (2)$$

Direct DFT Coupling Calculations. A representative set of 200 conformations was extracted from a GLYCAM simulation of **1**. Coupling constants were then computed for each of these conformers in the Gaussian 03 program²⁹ using the B3LYP functional³⁰ and the [5s2p1d3s1p] basis set.³⁵

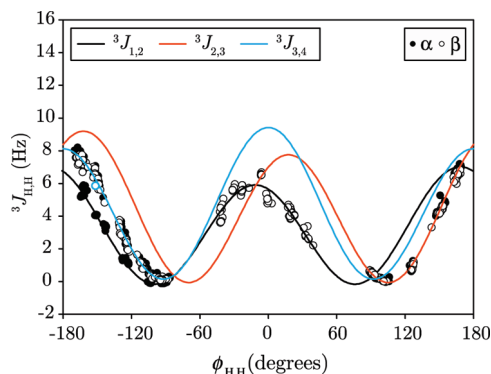


Figure 4. Karplus curves of $^3J_{1,2}$ (eq 3), $^3J_{2,3}$ (eq 4), and $^3J_{3,4}$ (eq 5) for methyl α -D-arabinofuranoside (filled circles, ●) and methyl β -D-arabinofuranoside (unfilled circles, ○) obtained from B3LYP/cc-pVTZ calculations.

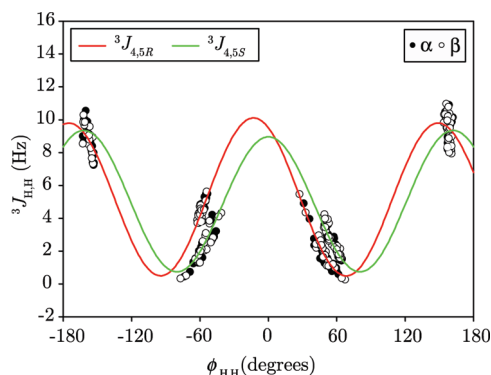


Figure 5. Karplus curves of $^3J_{4,5R}$ (eq 6) and $^3J_{4,5S}$ (eq 7) for methyl α -D-arabinofuranoside (filled circles, ●) and methyl β -D-arabinofuranoside (unfilled circles, ○).

The resulting $^3J_{H,H}$ values were then averaged over all 200 conformations.

Results and Discussion

Karplus Relationships for $^3J_{H,H}$ in D-Arabinofuranosides. In our previous report,⁸ Karplus equations were developed for methyl α -D-arabinofuranoside, the α -anomer of **1**. In the interest of generalization to all D-arabinofuranosides, Karplus relationships that can be applied to both α - and β -Araf residues were developed. To do this, $^3J_{H,H}$ values for both anomers of methyl D-arabinofuranoside were plotted together as a function of $\phi_{H,H}$. The data were fitted to obtain overall curves (Figures 4 and 5) and their corresponding parametrizations (eqs 3–7).

The ring protons display well-fitted curves (Figure 4 and eqs 3–5). The curve for $^3J_{3,4}$ is symmetrical about 0° and exhibits a global maximum of 10 Hz. In contrast, $^3J_{1,2}$ and $^3J_{2,3}$ curves are both shifted (nonsymmetry about 0°), and both required phase shifts for better fits (11° and -18° , respectively). In our previous report,⁸ the $^3J_{1,2}$ Karplus curve for α -Araf was not well parametrized around 0° because conformers with $\phi_{1,2}$ near 0° were not possible given the constraints of the ring system. With the addition of data points for **1**, this lack of parametrization at 0° has greatly improved.

$$^3J_{1,2}(\alpha, \beta) = 3.15 - 0.55 \cos(\phi + 11^\circ) + 3.30 \cos(2\phi + 22^\circ) \quad (R^2 = 0.98) \quad (3)$$

$$^3J_{2,3}(\alpha, \beta) = 4.21 - 0.72 \cos(\phi - 18^\circ) + 4.26 \cos(2\phi - 36^\circ) \quad (R^2 = 1.00) \quad (4)$$

$$^3J_{3,4}(\alpha, \beta) = 4.46 - 0.65 \cos(\phi) + 4.31 \cos(2\phi) \quad (R^2 = 0.99) \quad (5)$$

The exocyclic hydroxymethyl groups in both α - and β -Araf exhibit similar coupling profiles and well-fitted Karplus curves (Figure 5, eqs 6–7). The curve for $^3J_{4,5R}$ is shifted from the $^3J_{4,5S}$ curve, and a phase shift of 15° was added to ϕ for a better fit.

$$^3J_{4,5R}(\alpha, \beta) = 5.22 - 0.15 \cos(\phi + 15^\circ) + 4.73 \cos(2\phi + 30^\circ) \quad (R^2 = 0.97) \quad (6)$$

$$^3J_{4,5S}(\alpha, \beta) = 4.94 - 0.20 \cos(\phi) + 4.21 \cos(2\phi) \quad (R^2 = 0.97) \quad (7)$$

MD/DFT-determined $^3J_{H,H}$ in **1.** Using the DFT-derived relationships determined above, we computed averaged $^3J_{H,H}$ values using the distribution of conformers that were obtained from MD simulations of **1** using the GLYCAM04 carbohydrate parameter set. Presented in Table 1 (G04) is a comparison of these calculated $^3J_{H,H}$ values for **1** with those measured by NMR spectroscopy. The $^3J_{H,H}$ values computed using the conformer ensemble obtained from simulations using the GLYCAM06 force field are also included in Table 1 (G06).

Analysis of these data reveals that the combination of the MD conformer ensembles and the DFT-derived equations is able to reproduce experimental $^3J_{1,2}$ and $^3J_{4,5S}$ values with near perfect accuracy. However, as was observed in the analysis of α -arabinofuranosides,⁸ the computed $^3J_{4,5R}$ is underestimated compared with experiment (1.7 Hz deviation). This can be attributed to an underestimation of the gt rotamer population (i.e., the largest contributor to $^3J_{4,5R}$) by the MD simulations, which results in a lower overall average coupling constant.⁸ For **2–5**, similar trends are observed for $^3J_{4,5}$ values (see Table S-4 in the Supporting Information) with deviations ranging from 1.7–2.6 Hz for $^3J_{4,5R}$ and 0–0.6 Hz for $^3J_{4,5S}$.

Unlike in the α -Araf case,⁸ the calculated $^3J_{2,3}$ and $^3J_{3,4}$ couplings in the present β -Araf system also exhibit significant discrepancies compared to experimental values (deviations of 5.1 and 2.6 Hz, respectively). Analysis of the $^3J_{H,H}$ values obtained from the GLYCAM06 simulations reveals similar trends with slight improvements in the agreement of the ring couplings ($^3J_{1,2}$, $^3J_{2,3}$, and $^3J_{3,4}$).

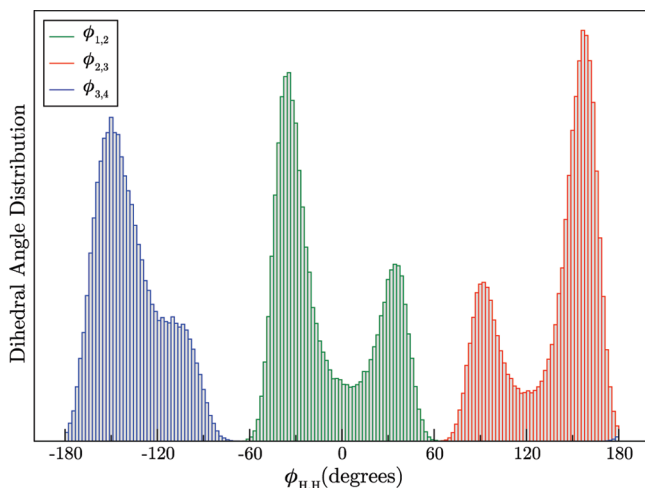
To investigate the source of the discrepancies in $^3J_{2,3}$ and $^3J_{3,4}$ values, the respective dihedral angle distributions ($\phi_{2,3}$ and $\phi_{3,4}$) obtained from MD simulations of **1** were examined (Figure 6); for comparison, the distribution of $\phi_{1,2}$ is also included in Figure 6.

For $\phi_{1,2}$, two populations are observed in the MD conformer ensemble, with the most populated angles observed at -32° (67%) and 36° (33%). The DFT-derived

Table 1. $^3J_{\text{H,H}}$ Values (in Hz) in **1** Obtained from Experiment and from MD Simulation Conformer Populations^a

	EXP	G04	G06	DDFT	B30	BIA	CHM	QMM	GRO
$^3J_{1,2}$	4.5	4.1	4.4	5.1	4.9	4.4	4.0	5.5	4.6
$^3J_{2,3}$	7.9	2.8	3.6	3.7	5.8	3.8	4.1	2.3	4.9
$^3J_{3,4}$	6.7	4.1	4.4	5.2	6.2	4.5	4.1	3.1	5.3
$^3J_{4,5\text{R}}$	6.7	5.1	5.0	5.7	4.5	4.9	5.0	6.4	4.8
$^3J_{4,5\text{S}}$	3.4	3.5	3.6	3.3	3.3	3.6	3.0	3.8	6.1

^aEXP = experimental values; G04 = using GLYCAM04 conformer ensemble; G06 = using GLYCAM06 conformer ensemble; DDFT = average $^3J_{\text{H,H}}$ from 200 conformations from MD conformer ensemble; B30 = using a biased set of conformers having P values in the range of -30° to 30° ; BIA = using conformer ensemble from simulations with biased set of atomic charges; CHM = using CHARMM conformer ensembles of **1**; QMM = using QM/MM conformer ensembles of **1**; and GRO = using GROMACS conformer ensembles of **1**.

**Figure 6.** Distributions of ring protons obtained from the GLYCAM06 MD simulations of **1**.

Karplus curve obtained for $^3J_{1,2}$ along with the two-population distribution for $\phi_{1,2}$ produce coupling constants that is in good agreement with experiment. In contrast, the distributions for $\phi_{2,3}$ and $\phi_{3,4}$ each exhibit two-state populations that negatively impact the value of the average $^3J_{\text{H,H}}$.

The most populated state for $\phi_{2,3}$ (72%) is centered at 160° and that for $\phi_{3,4}$ is centered on -148° (77%). Using the DFT-determined Karplus curves for these coupling fragments, these dihedral angle distributions give a relatively large coupling constant because the respective hydrogen atoms are in a near-trans relationship. However, the second population of conformers for both angles is centered near 90° (or -90° for $\phi_{3,4}$). These distributions produce coupling values that are near 0 Hz. Therefore, ensemble averaging over the two populations in each case results in a low overall $^3J_{\text{H,H}}$ value. These two-state populations are more heightened in the GLYCAM04 distributions (see Figure S-1 in the Supporting Information), where essentially identical populations are observed for the $\phi_{2,3}$ angle (55:45) and similar populations for $\phi_{3,4}$ (66:34) compared to the GLYCAM06 distributions. This is reflected in the worse agreement between the calculated and experimental $^3J_{2,3}$ and $^3J_{3,4}$ values with the conformer ensemble obtained from the GLYCAM04 simulations (Table 1, G04).

It should be noted that the major conformation about each of these angles ($\phi_{1,2} = -32^\circ$, $\phi_{2,3} = 160^\circ$, and $\phi_{3,4} = -148^\circ$) corresponds to conformers in the northern hemisphere of the pseudorotational wheel ($P = -31^\circ$ – 22°). These structures are similar to the major conformer of **1**, as determined earlier using the PSEUROT approach, which predicts a conformational equilibrium biased heavily ($\sim 90:10$) to a northern conformer (E_2/T_2 ; $P = -9$).¹⁰ This structure is also in good agreement with the conformation of the ring in the crystal structure of the molecule.⁵⁹ Thus, the simulations appear to predict the correct major conformer but underestimates its population in the conformational equilibrium.

Direct DFT $^3J_{\text{H,H}}$ Calculation. To evaluate whether the errors in $^3J_{\text{H,H}}$ values stem from the Karplus curve fitting procedure, we investigated a direct method that bypasses this step. Rather than fitting $\phi_{\text{H,H}}$ and $^3J_{\text{H,H}}$ data computed for each fragment in **1** and using the generated equations with the MD conformer ensembles, a representative set of conformers was instead chosen, and $^3J_{\text{H,H}}$ values were directly calculated for this set. Subsequently, the final $^3J_{\text{H,H}}$ values were obtained by averaging over all conformers in the set. Table 1 (DDFT) shows the $^3J_{\text{H,H}}$ values obtained from these calculations and their comparison to $^3J_{\text{H,H}}$ values from our original approach as well as to experiment.

In terms of the $^3J_{4,5}$ couplings, this direct approach shows better agreement with experiment. A comparison of C4–C5 rotamer distributions reveals that the same relative trend is observed in both conformer ensembles (gt > gg > tg); however, small differences are detected (45 gt: 15 tg: 40 gg using the full conformer set vs 51 gt: 11 tg: 38 gg for the 200 conformer set). This finding suggests that, although not ideal, the conformer distribution could be refined (by selecting “better” conformations) to more accurately reproduce the experimental result. Analysis of the ring couplings ($^3J_{1,2}$, $^3J_{2,3}$, and $^3J_{3,4}$) demonstrated that the direct DFT approach results in better agreement with experiment for $^3J_{3,4}$ values but in poorer agreement for $^3J_{1,2}$; no differences in agreement were observed between the two sets for $^3J_{2,3}$. These results suggest that this small set of conformers is not sufficient to properly represent the distribution of H–H dihedral angles along each coupling pathway. Although a closer value was observed for $^3J_{3,4}$, this may be fortuitous from the random selection of conformers for this set.

It is obvious from these results that proper sampling of conformers was not achieved; certain conformers were not sampled sufficiently and others more than desired. It is probable that a larger conformer set, or a more biased selection of the set, is required to obtain better agreement. This is, however, a rather unsatisfying approach, which requires insight into the conformation of the molecule before it is studied.

Langevin Thermostat Simulations. Given the results presented above, we reevaluated our previously employed protocol^{6–8} for carrying out the MD simulations of Araf rings. In addition to the simulations performed using the Berendsen thermostat (used in all our previous simulations), MD simulations of **1** were also carried out using the Langevin thermostat. However, upon analysis of the resulting conformer ensembles, negligible differences were observed in

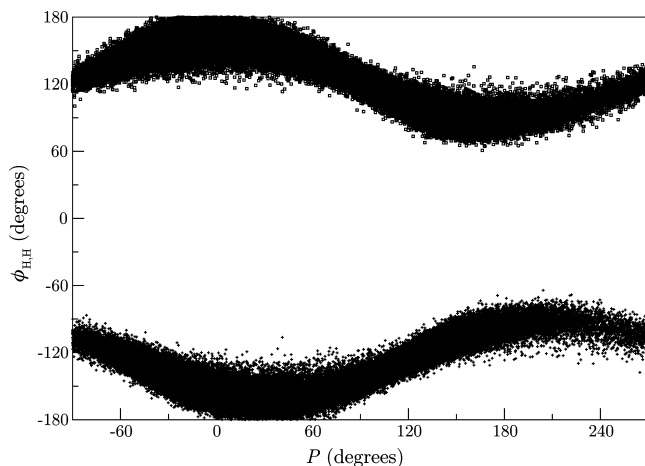


Figure 7. Plot of $\phi_{2,3}$ and $\phi_{3,4}$ as a function of P angle obtained from MD simulations of **1**.

both the rotamer populations as well as the distribution of ring conformations. For a discussion of the results, see Supporting Information (Figure S-2, Tables S-5 and S-6, and related discussion).

Biasing the MD Simulations. Further investigations to improve the predicted $^3J_{2,3}$ and $^3J_{3,4}$ values included the refinement of partial atomic charges to correspond to a biased set of conformations. In Figure 7, a plot of these couplings as a function of pseudorotational phase angle, P , is shown. In this plot, it can be seen that conformers that lie in the undesired $\phi_{2,3} = 90^\circ$ or $\phi_{3,4} = -90^\circ$ regions and give rise to $^3J_{H,H}$ near 0 Hz (Figure 6) correspond to P values in the southern hemisphere of the pseudorotational wheel (i.e., 90° – 270°), and the desired conformers are in the northern P range of -90° to 90° .

To assess whether better agreement in $^3J_{2,3}$ and $^3J_{3,4}$ values can be obtained if only a particular set of conformers is used for the charge calculations, we extracted all conformations that adopted a P value falling in the desired range of -30° to 30° from the entire 250 ns trajectory. Indeed, we observed significant improvements in $^3J_{H,H}$ when using these conformations compared with the use of the entire trajectory (Table 1, compare B30 and G06).

With this result in hand, we modified our atomic charge calculation procedure so that ensemble averaging of charges was performed on only the conformations that adopted preferred P values. This was done in the hope that these biased charges would lead to an improved MD conformer ensemble and therefore better agreement in $^3J_{H,H}$. However, when the MD simulation of **1** was carried out using this biased set of charges, similar conformer ensembles were observed compared to the unbiased case; $^3J_{H,H}$ values were, therefore, also similar (Table 1, BIA). This result essentially reiterates the highly flexible nature of these furanose systems. In fact, a time-dependence plot of the P angle (See Figure S-3 in Supporting Information) clearly indicates that even at short simulation times, all values of P can be readily visited (low-energy barriers); this is in contrast to the C4–C5 rotamers, which require long simulation times for proper sampling, especially the lower populated ones. These results are consistent with those previously described for MD

Table 2. MD Simulation Conformer Ensembles of **1** using the CHARMM Force Field

	C4–C5 rotamers ^a		ring conformation ^b		
	current	Hatcher et al. ⁵⁰		current	Hatcher et al. ⁵⁰
X_{gt}	45	64	P_N	-7°	-15°
X_{tg}	15	6	%N	60	62
X_{gg}	40	30	P_S	160°	183°
			%S	40	38

^a Experimental values: 57% gt, 8% tg, and 35% gg.

^b Experimental values: $P_N = -7^\circ$, 86%; $P_S = 162^\circ$, 14%.

simulations on arabinofuranosides^{6–8,60} as well as reported DFT calculations on these systems, which have revealed that the barrier to pseudorotation is small (~ 5 kcal/mol in the case of **1**)⁶¹ and lower than the energy required to rotate about the C4–C5 bond.⁶²

In light of the above results, we questioned whether the use of the GLYCAM force fields exhibited some limitations for their application to furanoses. Therefore, we explored three alternate methods for carrying out simulations of **1**: MD simulations using a furanose-specific force field⁵⁰ in the CHARMM program,⁴⁶ QM/MM simulations in the AMBER program,⁶³ and MD simulations using the GROMOS96 force field⁵⁶ in the GROMACS program.⁶⁴

Use of the CHARMM Force Field. In a recent report,⁵⁰ Hatcher et al. reported an additive all-atom empirical force field parametrized for aldopentofuranoses and their methyl glycosides as well as for fructofuranose rings. Exocyclic rotamer populations and puckering distributions were predicted from aqueous-phase MD simulations of both anomers of methyl D-arabinofuranoside. Therefore, we utilized this force field for our own simulations of **1** and found that we qualitatively reproduced the results reported by Hatcher et al. (Table 2). The C4–C5 rotamer populations follow the same trend, though differing percentages are observed. This discrepancy is likely a result of the length of the MD simulations. In our protocol, simulation times of ≥ 200 ns were carried out to ensure convergence of C4–C5 rotamer populations,^{6–8} whereas 20 ns simulations were employed in the Hatcher et al. report.⁵⁰ With regards to ring conformation, our simulations predicted north and south conformer populations that are almost identical to those previously reported⁵⁰ with the most populated conformers differing slightly.

With the MD conformer ensemble from the CHARMM simulations in hand, we carried out $^3J_{H,H}$ calculations as before, and the results are presented in Table 1 (CHM). This analysis reveals that, although slightly better agreement in $^3J_{2,3}$ is observed (4.1 Hz compared to 3.6 Hz), the remaining coupling constants exhibit similar or slightly worse agreement with experiment compared to those calculated with the GLYCAM06 conformer distributions. This discrepancy again can be attributed to the large percentage of southern conformers predicted by the simulations that correspond to near perpendicular $\phi_{2,3}$ and $\phi_{3,4}$ dihedral angles (see Figures S-3 and S-4 in the Supporting Information for a plot of the distributions). The near zero couplings resulting from these conformers give rise to a low overall $^3J_{H,H}$.

QM/MM Simulations of 1. The next method attempted toward a potential solution to the discrepancies in predicted

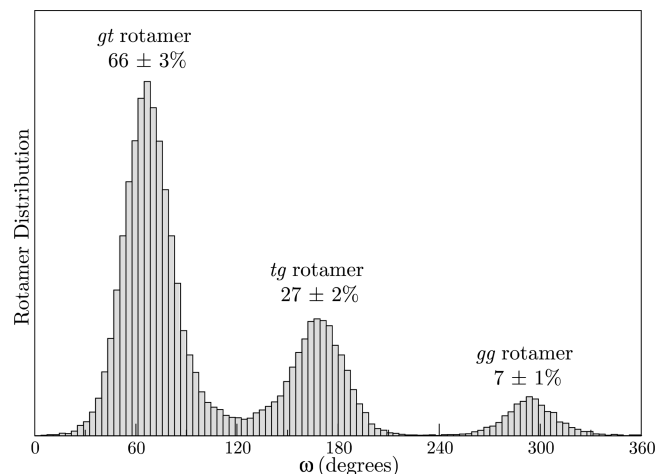


Figure 8. Histogram plot of the C4–C5 rotamer distributions obtained from QM/MM simulations of **1**.

$^3J_{\text{H,H}}$ values involved the use of a combined QM/MM approach where **1** was treated using QM, and the solvent was modeled with MM. The PM3CARB-1 parameter set was used in these simulations as it has shown improved prediction of intramolecular hydrogen-bond strength, ring conformation, and energetics compared to PM3.^{53,54} In previous reports, this parameter set was used to accurately predict hydroxymethyl group conformation in gluco- and galactopyranose using QM/MM simulations⁵⁴ as well as adequate prediction of glycosidic linkage conformation in three disaccharides: (β -D-glucopyranosyl-(1 \rightarrow 4)- β -D-glucopyranose, α -D-glucopyranosyl-(1 \rightarrow 4)- α -D-glucopyranose, and α -D-galactopyranosyl-(1 \rightarrow 4)- α -D-galactopyranose).⁶⁵

Using the same convergence criteria as we employed previously (i.e., errors of $\leq 3\%$ in C4–C5 rotamer populations), we observed that a simulation time of 100 ns was sufficient for proper convergence in these QM/MM simulations (see Figure S-6 in the Supporting Information for convergence plot). Figure 8 shows a histogram of the resulting rotamer distributions about the C4–C5 bond in **1**.

Integration of the peaks in the histogram produces a distribution of 66:27:7 for the gt:tg:gg rotamers. Unlike in previous MD simulations of **1**, this trend in the populations (gt > tg > gg) contradicts the experimental result (gt > gg > tg). The gg rotamer is found to be the least populated, indicating that the gauche effect,⁶⁶ the preference for adjacent electronegative substituents along a two-carbon fragment to adopt the gauche orientation, is not properly considered in the calculations. Moreover, hydrogen-bond analysis of the resulting conformer ensemble (see Table S-7 in the Supporting Information) showed no significant occupancy of intramolecular hydrogen bonds.

Upon analysis of the $^3J_{\text{H,H}}$ using the B3LYP/cc-pVTZ-determined Karplus equations with the conformer ensemble from the QM/MM simulations, we observed excellent agreement in the $^3J_{4,5}$ couplings (Table 1, QMM). This result suggests errors in the experimental model used to calculate rotamer populations. Having correctly reproduced the $^3J_{4,5}$ obtained from NMR spectroscopy, it would appear that these QM/MM simulations are the ideal choice for determining the hydroxymethyl group conformation in this system.

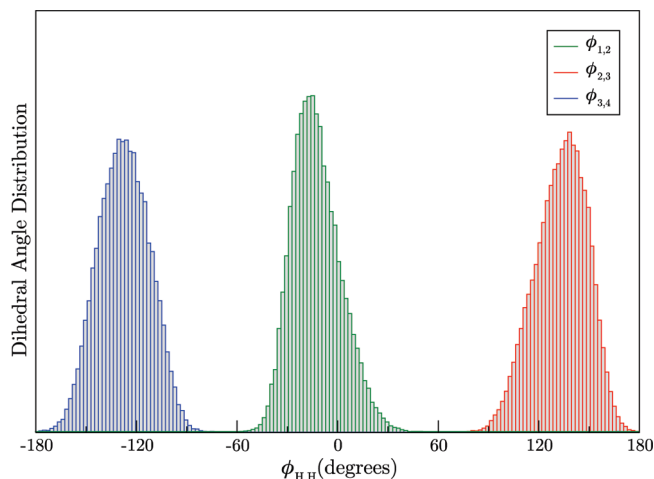


Figure 9. Distributions of ring protons obtained from the QM/MM simulations of **1**.

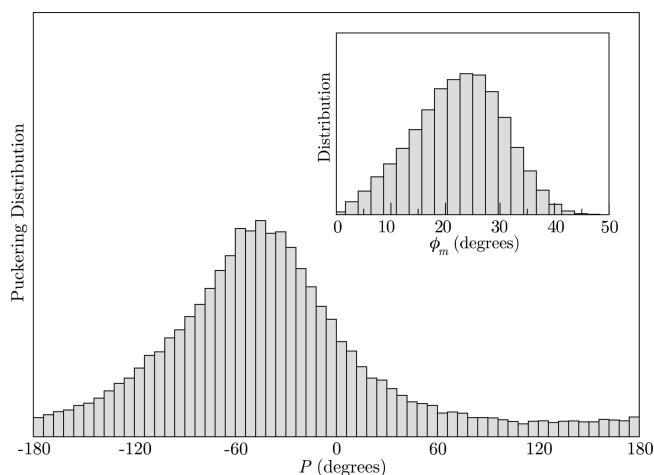


Figure 10. Distribution of the pseudorotational phase angle, P , and the puckering amplitude, ϕ_m (inset), obtained from QM/MM simulations of **1**.

However, as will be seen later when more accurate Karplus equations are used, this is not the case.

Analysis of the ring $^3J_{\text{H,H}}$ (Table 1, QMM) revealed much worse agreement with experiment than those calculated from the other MD simulations. To understand this discrepancy, we again looked at the dihedral angle distributions of the ring protons obtained from these QM/MM simulations (Figure 9). For all ring protons, the $\text{H}_x\text{--C}_x\text{--C}_{x+1}\text{--H}_{x+1}$ distributions each exhibit single-state populations, which is in contrast to what was observed in the classic MD simulations (See Figure 6).

For $\phi_{1,2}$, the distribution is centered about -13° , which corresponds to a larger $^3J_{1,2}$ than observed in experiment (see Karplus curve for $^3J_{1,2}$, above). Similarly, the distributions of $\phi_{2,3}$ and $\phi_{3,4}$ show the most probable dihedral angles at 140° and -127° , respectively, both of which correspond to low $^3J_{\text{H,H}}$ values (2.7 and 2.9 Hz, respectively). Upon examination of the distributions of ring conformations (Figure 10), the source of these discrepancies in the dihedral angle distributions became clear.

The distribution of P produces an average of -37° that corresponds to a conformation in the northwestern region

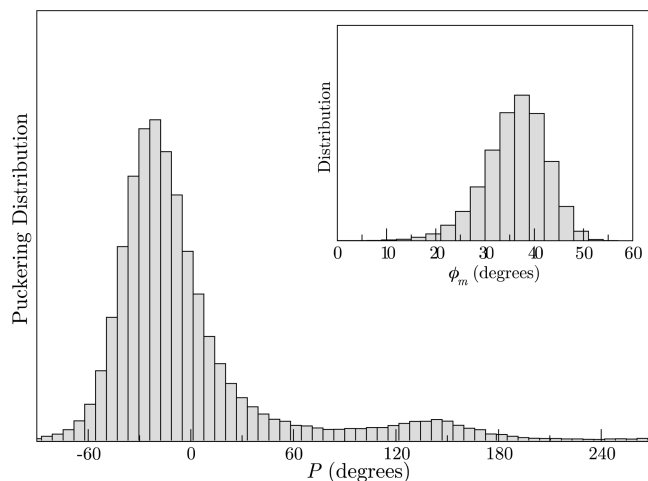


Figure 11. Distribution of the pseudorotational phase angle, P , and the puckering amplitude, ϕ_m (inset), obtained from GROMACS simulations of **1**.

of the pseudorotational wheel ($^1E/{}^1T_2$). This value is comparable to the northern P values predicted from the other simulations. More interestingly, however, is the predicted puckering amplitude, ϕ_m , which gives an average of 22° . A statistical analysis of a large number of β -D-furanoside X-ray structures suggest the β -Araf ring adopts an optimal ϕ_m of 38° .^{59,67} Therefore the QM/MM simulations predict a ring that is too flat, which we propose results in undesired ring H–C–C–H dihedral angle distributions. From these results, we can conclude that although the use of PM3CARB-1 in QM/MM simulations of **1** appears to correctly predict hydroxymethyl group conformation, it is not sufficient for determining ring conformation in **1**.

GROMACS Simulations of 1. In a recent report, unconstrained MD simulations of 2-*O*-sulfo- α -L-iduronic acid (IdoA2S) were carried using the GLYCAM06 and GROMOS96 force fields to investigate their ability to reproduce conformational distributions of the idopyranose ring, another flexible monosaccharide.^{68–71} It was found that the predicted ring conformation using GROMOS96 was in better agreement with experiment than the use of the GLYCAM06 force field. Moreover, the predicted hydroxymethyl group conformation was similar in both cases. Therefore, to probe its performance in our systems, the GROMOS96 force field was utilized in MD simulations of **1**.

The resulting distribution of ring conformations as well as the C4–C5 rotamer populations is presented in Figures 11 and 12, respectively. Analysis of the puckering (Figure 11) shows a heavily biased distribution (92%) of northern conformers centered about $P_N = -14^\circ$ and a small population (8%) of southern conformers centered on $P_S = 144^\circ$. Moreover, the predicted puckering amplitude agrees well with previous simulations (with the exception of QM/MM), DFT theory calculations,¹¹ and X-ray data.⁵⁹

Analysis of the ring ${}^3J_{H,H}$ values (Table 1, GRO) shows that with this puckering distribution, we indeed observe better agreement with experiment compared to the other simulations. Although the ${}^3J_{2,3}$ and ${}^3J_{3,4}$ values remain too small, the resulting values are now much closer to experiment

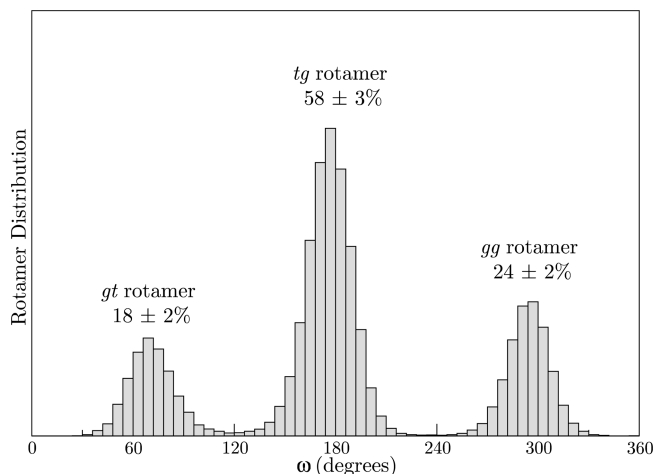


Figure 12. Histogram plot of the C4–C5 rotamer distributions obtained from GROMACS simulations of **1**.

compared to the other simulations, and we observe near perfect agreement in ${}^3J_{1,2}$.

Upon analysis of ${}^3J_{4,5}$, however, we observe significant deviation from experiment; the predicted values are now in reverse order. This result can be explained in a similar manner to that reported previously.⁸ Looking at the C4–C5 rotamer distributions obtained from the MD simulations (Figure 12), it can be seen that the tg rotamer is predicted to be the most populated (58%). This rotamer is the largest contributor to ${}^3J_{4,5S}$, as opposed to the gt rotamer which produces the largest ${}^3J_{4,5R}$. Hence, the observed trend in ${}^3J_{4,5}$ couplings is a result of significant overestimation of the tg rotamer by the MD simulations.

More Accurate DFT Coupling Profiles. The significantly lower magnitudes in ${}^3J_{2,3}$ and ${}^3J_{3,4}$ compared to experiment prompted reinvestigation of the Karplus relationships calculated for the β -Araf system. Upon analysis of all coupling constants calculated using the B3LYP/cc-pVTZ level of theory, we discovered that the maximum ${}^3J_{2,3}$ value that could be obtained was 6.8 Hz. This indicated that, regardless of which conformer ensemble is chosen, the predicted ${}^3J_{2,3}$ will not likely reach the experimental value of 7.9 Hz. Therefore, additional coupling profiles for **1** were computed using DFT calculations and an augmented basis set (aug-cc-pVTZ-J). This basis set has been optimized for calculation of spin–spin coupling constants and has been shown to produce accurate one-, two-, and three-bond J values in a number of small molecules containing electronegative substituents.³⁴ The spin–spin coupling constant data calculated using this augmented basis set were plotted as a function of the respective H–C–C–H torsion angles and fitted to eq 1 (the resulting curves along with their parametrizations are presented in the Supporting Information, Figure S-12 and equations S-1–5).

With these revised Karplus relationships in hand, we carried out calculations of averaged ${}^3J_{H,H}$ values using the distribution of conformers from all previous simulations of **1**. Analysis of the resulting data (Table 3, A) clearly shows that, overall, the ${}^3J_{H,H}$ magnitudes are larger than those obtained using the original DFT-derived Karplus relationships (eqs 3–7). In general, there is good agreement with

Table 3. $^3J_{\text{H,H}}$ Values (in Hz) for **1** using DFT-Derived Karplus Curves with Various MD Conformer Ensembles^a

	EXP	G04	G06	CHM	QMM	GRO
A B3LYP/aug-cc-pVTZ-J-Derived Karplus Curves						
$^3J_{1,2}$	4.5	4.9	5.1	4.7	6.7	5.4
$^3J_{2,3}$	7.9	3.5	4.6	5.3	2.9	6.3
$^3J_{3,4}$	6.7	5.2	5.5	5.1	3.8	6.6
$^3J_{4,5\text{R}}$	6.7	6.3	6.1	6.2	7.9	5.6
$^3J_{4,5\text{S}}$	3.4	4.0	4.1	3.3	4.5	7.4
B B3LYP/5s2p1d3s1p-Derived Karplus Curves						
$^3J_{1,2}$	4.5	4.6	4.9	4.5	6.2	5.1
$^3J_{2,3}$	7.9	3.2	4.3	4.8	2.6	5.9
$^3J_{3,4}$	6.7	4.8	5.1	4.8	3.4	6.2
$^3J_{4,5\text{R}}$	6.7	5.8	5.7	5.8	7.4	5.3
$^3J_{4,5\text{S}}$	3.4	3.7	3.8	3.2	4.2	7.0

^aEXP = experimental values; G04 = using GLYCAM04 conformer ensembles of **1**; G06 = using GLYCAM06 conformer ensembles of **1**; CHM = using CHARMM conformer ensembles of **1**; QMM = using QM/MM conformer ensembles of **1**; and GRO = using GROMACS conformer ensembles of **1**.

experiment for $^3J_{1,2}$ (with the exception of QM/MM) and $^3J_{4,5\text{S}}$ (with the exception of GROMACS). Moreover, both of the GLYCAM and the CHARMM simulations predict comparatively accurate $^3J_{4,5\text{R}}$ values.

Overall, there is generally better agreement in $^3J_{2,3}$ and $^3J_{3,4}$ values; however, significant underestimation of the magnitudes remains. The GROMACS simulations predict the closest $^3J_{2,3}$ and $^3J_{3,4}$ values, although the trend remains in reverse compared to experiment, and $^3J_{1,2}$ has deviated away from the experimental value. Moreover, as discussed above, the GROMACS-predicted $^3J_{4,5}$ couplings are inconsistent with experiment.

The QM/MM simulations provide the worst agreement overall; using these new Karplus relationships, not a single $^3J_{\text{H,H}}$ shows reasonable agreement. In contrast, the best agreement in $^3J_{1,2}$, $^3J_{4,5\text{R}}$, and $^3J_{4,5\text{S}}$, and the correct trend in $^3J_{2,3}$ and $^3J_{3,4}$ is provided by the CHARMM simulations. For the sake of completeness, we also used Karplus equations using the Serianni–Carmichael [5s2p1d3s1p] basis set to calculate $^3J_{\text{H,H}}$. In fact, similar results compared to the augmented basis set were obtained using this basis set (Table 3, B).

Conclusions

We report here the combined use of conformer ensembles obtained from MD simulations and DFT-derived Karplus relationships for subsequent calculation of $^3J_{\text{H,H}}$ ($^3J_{1,2}$, $^3J_{2,3}$, $^3J_{3,4}$, $^3J_{4,5\text{R}}$, and $^3J_{4,5\text{S}}$) as a conformational probe. This approach allows for the direct comparison of vicinal coupling constants obtained from NMR spectroscopy, thereby avoiding possible sources of errors encountered in the models used to analyze NMR data (e.g., the two-state model inherent in PSEUROT¹⁵ or the “discrete” model).⁷²

The coupling constant values calculated from the DFT-derived $^3J_{\text{H,H}}$ relationships for α -Araf residues, as reported previously,⁸ showed reasonable agreement with experiment. This result reiterates the ability of the AMBER/GLYCAM simulations to provide accurate conformer distributions of

oligosaccharides containing α -Araf rings. However, studies on the β -Araf system using this approach displayed a number of difficulties.

Conformer ensembles obtained from MD simulations using the GLYCAM04 parameter set and the GLYCAM06 force field were used to calculate $^3J_{\text{H,H}}$ in **1**. The results show that reasonable agreement can be obtained for $^3J_{1,2}$ and $^3J_{4,5}$, but significant deviations are observed for $^3J_{2,3}$ and $^3J_{3,4}$. To understand this discrepancy, we evaluated the dihedral angle distributions predicted by the MD simulations along these fragments and found that a large population of conformers adopt near perpendicular $\phi_{2,3}$ and $\phi_{3,4}$ angles, which result in negligible $^3J_{\text{H,H}}$ values. These distributions arise from ring conformations that are present in the southern region of the pseudorotational wheel, which, on the basis of previous experimental work,^{10,61,73} appear to be populated only to a small degree in solution. In fact, an analysis of $^3J_{\text{H,H}}$ for northern conformers showed significant improvements for the ring couplings over the use of the entire trajectory. However, when a set of northern-biased partial atomic charges was used in MD simulations of **1**, no change in the distribution of puckering was observed.

To find a potential solution to the discrepancy in $^3J_{\text{H,H}}$, we explored a direct DFT method, which avoids generating Karplus equations and instead calculates $^3J_{\text{H,H}}$ from a representative set of conformations. We envisioned that this protocol would circumvent any errors that may be introduced in the fitting procedure. The resulting $^3J_{\text{H,H}}$ from this method showed slightly better agreement with experiment, in general. A larger set of conformers may be required to accurately represent the phase space of this molecule. However, as the numbers of conformers required for good agreement with experiment increases, the practicality of this approach decreases due to the large cost of the DFT spin–spin coupling calculations. Potentially, the MD conformer ensemble can be tailored so as to reproduce the experimental data. This is, in principle, similar to a time-averaged restrained molecular dynamics (tar-MD) simulation where NMR restraints are used to bias the simulation to reproduce experimental data. This procedure was, in fact, recently used to study the conformation of a number of ribofuranose-based molecules.¹⁹ However, this requires prior knowledge of NMR data and therefore would be insufficient for large oligosaccharides where experimental data can be difficult to obtain, due to spectral overlap. Furthermore, use of these approaches may hinder the development of an unbiased and general model to accurately probe the conformational preferences of these Araf systems.

Different force fields were also investigated in simulations of **1** for their ability to predict accurate conformer ensembles. The recently developed CHARMM force field for aldopentofuranosides⁵⁰ predicted average $^3J_{\text{H,H}}$ values that were in similar agreement with experiment compared to GLYCAM06. The predicted C4–C5 rotamer populations as well as ring conformer distributions were similar to those reported by Hatcher et al.⁵⁰ Use of the GROMOS96 force field showed $^3J_{2,3}$ and $^3J_{3,4}$ values that are closer to experiment than those predicted by CHARMM, but the couplings along the C4–C5 fragment deviated significantly. The

predicted conformation of the hydroxymethyl group showed a distribution of 18:58:24 for gt:tg:gg. This result is peculiar, as the tg rotamer (which is the most populated in this case) lacks any stabilizing stereoelectronic effects that are present in the gt or gg rotamers, such as the gauche effect or intramolecular hydrogen bonds. Recent investigations on IdoA2S conformation showed that both GROMOS96 and GLYCAM06 force field are able to accurately predict hydroxymethyl group conformation.⁷⁴ In our simulations, however, these two force fields predict significantly different conformer distributions.

QM/MM simulations of **1** showed conflicting results. With the original DFT Karplus equations (from the B3LYP/cc-pVTZ calculations), these simulations appeared to have correctly predicted the hydroxymethyl group conformation. However, with the use of the augmented basis set or the Serianni–Carmichael basis set, both of which gave reasonable agreements using the classical MD conformer ensembles, the semiempirical QM/MM simulations resulted in contradictory results. It is possible that a different QM theory (other than PM3CARB-1) may be needed for better agreement. Alternatively, a DFT-MD approach that was recently applied to study the conformation of glucopyranose and all its epimers⁷⁵ may also be useful in this system. However, the use of this methodology for larger systems (such as **2–5**) is not practical from a computational perspective.

A final attempt at obtaining accurate $^3J_{\text{H,H}}$ from MD conformer ensembles involved the reevaluation of the DFT-derived Karplus equations. In the earlier work on α -Araf-containing molecules, the coupling profiles generated using the Dunning cc-pVTZ basis set proved to be sufficient for predicting $^3J_{\text{H,H}}$.⁸ However, for the present β -Araf case, an augmented basis set (aug-cc-pVTZ-J) was required to obtain closer $^3J_{\text{H,H}}$ values; similar agreement was also observed using the Serianni–Carmichael [5s2p1d1s1p] basis set. In comparison, use of the Serianni–Carmichael basis set offers a more superior method in terms of its relatively smaller size, and therefore, its more efficient calculation of spin–spin coupling profiles. In both cases, the CHARMM simulations appear to provide the best agreement in $^3J_{\text{H,H}}$ with experiment, although significant deviations were still observed, and GLYCAM06 performs similarly.

In conclusion, the range of simulation methods used here to model the β -Araf ring demonstrated that the conformer populations obtained predict ^1H – ^1H vicinal coupling constants that were in less good agreement with experiment, compared to previous investigations of α -Araf rings. It is, of course, possible that other fixed charged force field models not attempted here, such as MM4,^{76,77} could result in better agreement with experiment. Moreover, reparameterization of force field torsional functions may also be performed to obtain possibly better conformer distributions and work in this direction is currently underway. Other possibilities include the use of polarizable force field models to capture electronic polarization effects. The use of such force fields has not been required in the case of oligosaccharides containing pyranose residues.^{78–82} However, as shown in previous reports,^{6,7} fluctuations in fixed partial atomic charges in five-membered rings can change significantly as

a function of ring pucker of both α - and β -Araf rings, and therefore, inclusion of polarization in the model may result in better prediction of ring conformation. Models that include explicit treatment of electronic polarizability have been developed that can be used to treat alcohols.^{83–88} Polarizable empirical force fields that are based on the classical Drude model^{86,88} have also been reported for primary and secondary alcohols⁸⁹ as well as for linear and cyclic ethers.⁹⁰ Moreover, a general purpose polarizable model, AMOEBA, which replaces the fixed partial charge model with polarizable atomic multipoles through the quadrupole moments, has also been recently developed.⁹¹ Therefore, we anticipate that a more accurate electrostatic representation together with force field torsional reparameterization would benefit the depiction of the conformational preferences of both α - and β -Araf systems.

Acknowledgment. This work was supported by the Alberta Ingenuity Centre for Carbohydrate Science and the Natural Sciences and Engineering Research Council of Canada. H.A.T. thanks the Province of Alberta for a Queen Elizabeth II scholarship.

Supporting Information Available: Coupling constant data for Karplus curve fitting, biased partial atomic charges for **1**, $^3J_{\text{H,H}}$ values in **2–5**, couplings for different thermostats, time dependence of P , conformer distributions from CHARMM and QM/MM simulations, H-bond analysis from QM/MM simulations, and more accurate Karplus equations. This information is available free of charge via the Internet at <http://pubs.acs.org>.

References

- (1) Brennan, P. J.; Nikaido, H. *Annu. Rev. Biochem.* **1995**, *64*, 29.
- (2) de Lederkremer, R. M.; Colli, W. *Glycobiology* **1995**, *5*, 547.
- (3) Peltier, P.; Euzen, R.; Daniellou, R.; Nugier-Chauvin, C.; Ferrières, V. *Carbohydr. Res.* **2008**, *343*, 1897.
- (4) Richards, M. R.; Lowary, T. L. *ChemBioChem* **2009**, *10*, 1920.
- (5) Lowary, T. L. *Curr. Opin. Chem. Biol.* **2003**, *7*, 749.
- (6) Seo, M.; Castillo, N.; Ganzynkiewicz, R.; Daniels, C. R.; Woods, R. J.; Lowary, T. L.; Roy, P.-N. *J. Chem. Theory Comput.* **2008**, *4*, 184.
- (7) Taha, H. A.; Castillo, N.; Roy, P.; Lowary, T. L. *J. Chem. Theory Comput.* **2009**, *5*, 430.
- (8) Taha, H. A.; Castillo, N.; Sears, D. N.; Wasylishen, R. E.; Lowary, T. L.; Roy, P. *J. Chem. Theory Comput.* **2010**, *6*, 212.
- (9) Brennan, P. J. *Tuberculosis* **2003**, *83*, 91.
- (10) Houseknecht, J.; Altona, C.; Hadad, C. M.; Lowary, T. L. *J. Org. Chem.* **2002**, *67*, 4647.
- (11) Houseknecht, J.; Lowary, T. L.; Hadad, C. M. *J. Phys. Chem. A* **2003**, *107*, 5763.
- (12) Homans, S. W. Conformational Analysis in Solution by NMR. In *Carbohydrates in Chemistry and Biology*; Ernst, B., Hart, G. W., Sinay, P., Eds.; Wiley-VCH: New York, 2000; pp 947.

- (13) Jimenez-Barbero, J.; Diaz, M. D.; Nieto, P. M. *Anti-Cancer Agents Med. Chem.* **2008**, 8, 52.
- (14) Kato, K.; Sasakawa, H.; Kamiya, Y.; Utsumi, M.; Nakano, M.; Takahashi, N.; Yamaguchi, Y. *Biochim. Biophys. Acta* **2008**, 1780, 619.
- (15) de Leeuw, F. A. A. M.; Altona, C. *J. Comput. Chem.* **1983**, 4, 428.
- (16) Hendrickx, P. M. S.; Martins, J. C. *Chem. Cent. J.* **2008**, 2, 20.
- (17) Thibaudeau, C.; Kumar, A.; Bekiroglu, S.; Matsuda, A.; Marquez, V. E.; Chattopadhyaya, J. *J. Org. Chem.* **1998**, 63, 5447.
- (18) Barchi, J. J.; Karki, R. G.; Nicklaus, M. C.; Siddiqui, M. A.; George, C.; Mikhailopulo, I. A.; Marquez, V. E. *J. Am. Chem. Soc.* **2008**, 130, 9048.
- (19) Hendrickx, P.; Corzana, F.; Depraetere, S.; Tourwe, D.; Augustyns, K.; Martins, J. *J. Comput. Chem.* **2010**, 31, 561.
- (20) Plavec, J.; Koole, L. H.; Chattopadhyaya, J. *J. Biochem. Biophys. Methods* **1992**, 25, 253.
- (21) Schlesinger, L. S. *Curr. Top. Microbiol. Immunol.* **1996**, 215, 71.
- (22) Nigou, J.; Gilleron, M.; Puzo, G. *Biochimie* **2003**, 85, 153.
- (23) Chatterjee, D.; Lowell, K.; Rivoire, B.; McNeil, M. R.; Brennan, P. J. *J. Biol. Chem.* **1992**, 267, 6234.
- (24) Chatterjee, D.; Roberts, A. D.; Lowell, K.; Brennan, P. J.; Orme, I. M. *Infect. Immun.* **1992**, 60, 1249.
- (25) Chatterjee, D.; Bozic, C. M.; McNeil, M.; Brennan, P. J. *J. Biol. Chem.* **1991**, 266, 9652.
- (26) Rademacher, C.; Shoemaker, G.; Kim, H.; Zheng, R.; Taha, H. A.; Liu, C.; Nacario, R.; Schriemer, D.; Klassen, J. S.; Peters, T.; Lowary, T. L. *J. Am. Chem. Soc.* **2007**, 129, 10489.
- (27) Murase, T.; Zheng, R. B.; Joe, M.; Bai, Y.; Marcus, S. L.; Lowary, T. L.; Ng, K. K. S. *J. Mol. Biol.* **2009**, 392, 381.
- (28) Altona, C.; Francke, R.; de Haan, R.; Ippel, J. H.; Daalman, G. J.; Hoekzema, A. J. A. W.; van Wijk, J. *Magn. Reson. Chem.* **1994**, 32, 670.
- (29) Frisch, M. J.; Trucks, G. W.; Schlegel, H. B.; Scuseria, G. E.; Robb, M. A.; Cheeseman, J. R.; Montgomery, J. A., Jr.; Vreven, T.; Kudin, K. N.; Burant, J. C.; Millam, J. M.; Iyengar, S. S.; Tomasi, J.; Barone, V.; Mennucci, B.; Cossi, M.; Scalmani, G.; Rega, N.; Petersson, G. A.; Nakatsuji, H.; Hada, M.; Ehara, M.; Toyota, K.; Fukuda, R.; Hasegawa, J.; Ishida, M.; Nakajima, T.; Honda, Y.; Kitao, O.; Nakai, H.; Klene, M.; Li, X.; Knox, J. E.; Hratchian, H. P.; Cross, J. B.; Bakken, V.; Adamo, C.; Jaramillo, J.; Gomperts, R.; Stratmann, R. E.; Yazyev, O.; Austin, A. J.; Cammi, R.; Pomelli, C.; Ochterski, J. W.; Ayala, P. Y.; Morokuma, K.; Voth, G. A.; Salvador, P.; Dannenberg, J. J.; Zakrzewski, V. G.; Dapprich, S.; Daniels, A. D.; Strain, M. C.; Farkas, O.; Malick, D. K.; Rabuck, A. D.; Raghavachari, K.; Foresman, J. B.; Ortiz, J. V.; Cui, Q.; Baboul, A. G.; Clifford, S.; Cioslowski, J.; Stefanov, B. B.; Liu, G.; Liashenko, A.; Piskorz, P.; Komaromi, I.; Martin, R. L.; Fox, D. J.; Keith, T.; Al-Laham, M. A.; Peng, C. Y.; Nanayakkara, A.; Challacombe, M.; Gill, P. M. W.; Johnson, B.; Chen, W.; Wong, M. W.; Gonzalez, C.; and Pople, J. A. *Gaussian 03*, revision E.01; Gaussian, Inc.: Wallingford, CT, 2004.
- (30) Becke, A. D. *J. Chem. Phys.* **1993**, 98, 5648.
- (31) Helgaker, T.; Watson, M.; Handy, N. *J. Chem. Phys.* **2000**, 113, 9402.
- (32) Dunning, T. H., Jr. *J. Chem. Phys.* **1989**, 90, 1007.
- (33) Kendall, R. A.; Dunning, T. H.; Harrison, R. J. *J. Chem. Phys.* **1992**, 96, 6796.
- (34) Provasi, P. F.; Aucar, G. A.; Sauer, S. P. A. *J. Chem. Phys.* **2001**, 115, 1324.
- (35) Stenutz, R.; Carmichael, I.; Widmalm, G.; Serianni, A. S. *J. Org. Chem.* **2002**, 67, 949.
- (36) Marquardt, D. W. *J. Soc. Ind. Appl. Math.* **1963**, 11, 431.
- (37) Haasnoot, C.; de Leeuw, F.; Altona, C. *Tetrahedron* **1980**, 36, 2783.
- (38) Case, D. A.; Darden, T. A.; T.E. Cheatham, I.; Simmerling, C. L.; Wang, J.; Duke, R. E.; Luo, R.; Crowley, M.; Walker, R. C.; Zhang, W.; Merz, K. M.; Wang, B. Hayik, S.; Roitberg, A.; Seabra, G.; Kolossváry, I.; Wong, K. F. Paesani, F.; Vanicek, J.; Wu, X. Brozell, S. R.; Steinbrecher, T.; Gohlke, H.; Yang, L.; Tan, C.; Mongan, J.; Hornak, V.; Cui, G.; Mathews, D. H.; Seetin, M. G.; Sagui, C.; Babin, V.; Kollman, P. A. *AMBER 10*, University of California: San Francisco, 2008.
- (39) Woods, R. J.; Dwek, R.; Edge, C.; Fraser-Reid, B. *J. Phys. Chem.* **1995**, 99, 3832.
- (40) Ryckaert, J.; Ciccotti, G.; Berendsen, H. *J. Comput. Phys.* **1977**, 23, 327.
- (41) Berendsen, H. J. C.; Postma, J. P. M.; van Gunsteren, W. F.; Dinola, A.; Haak, J. R. *J. Chem. Phys.* **1984**, 81, 3684.
- (42) Darden, T.; York, D.; Pedersen, L. *J. Chem. Phys.* **1993**, 98, 10089.
- (43) Essmann, U.; Perera, L.; Berkowitz, M. L.; Darden, T.; Lee, H.; Pedersen, L. G. *J. Chem. Phys.* **1995**, 103, 8577.
- (44) Kirschner, K. N.; Yongye, A. B.; Tschampel, S. M.; Gonzalez-Outeirino, J.; Daniels, C. R.; Foley, B. L.; Woods, R. J. *J. Comput. Chem.* **2008**, 29, 622.
- (45) Adelman, S. A.; Doll, J. D. *J. Chem. Phys.* **1976**, 64, 2375.
- (46) Brooks, B. R.; Brooks, C. L.; Mackerell, A. D.; Nilsson, L.; Petrella, R. J.; Roux, B.; Won, Y.; Archontis, G.; Bartels, C.; Boresch, S.; Caflisch, A.; Caves, L.; Cui, Q.; Dinner, A. R.; Feig, M.; Fischer, S.; Gao, J.; Hodoscek, M.; Im, W.; Kucsera, K.; Lazaridis, T.; Ma, J.; Ovchinnikov, V.; Paci, E.; Pastor, R. W.; Post, C. B.; Pu, J. Z.; Schaefer, M.; Tidor, B.; Venable, R. M.; Woodcock, H. L.; Wu, X.; Yang, W.; York, D. M.; Karplus, M. *J. Comput. Chem.* **2009**, 30, 1545.
- (47) Hoover, W. G. *Phys. Rev. A* **1985**, 31, 1695.
- (48) Nosé, S. *Mol. Phys.* **1984**, 52, 255.
- (49) Feller, S. E.; Zhang, Y.; Pastor, R. W.; Brooks, B. R. *J. Chem. Phys.* **1995**, 103, 4613.
- (50) Hatcher, E.; Guvench, O.; MacKerell, A. D. *J. Phys. Chem. B* **2009**, 113, 12466.
- (51) Miller, B. T.; Singh, R. P.; Klauda, J. B.; Hodošček, M.; Brooks, B. R.; Woodcock, H. L. *J. Chem. Inf. Model.* **2008**, 48, 1920.
- (52) Jorgensen, W. L.; Chandrasekhar, J.; Madura, J. D.; Impey, R. W.; Klein, M. L. *J. Chem. Phys.* **1983**, 79, 926.
- (53) McNamara, J. P.; Muslim, A. M.; Abdel-Aal, H.; Wang, H.; Mohr, M.; Hillier, I. H.; Bryce, R. A. *Chem. Phys. Lett.* **2004**, 394, 429.

- (54) Barnett, C. B.; Naidoo, K. J. *J. Phys. Chem. B* **2008**, *112*, 15450.
- (55) van der Spoel, D.; Lindahl, E.; Hess, B.; Groenhof, G.; Mark, A. E.; Berendsen, H. J. *Comput. Chem.* **2005**, *26*, 1701.
- (56) van Gunsteren, W. F.; Billeter, S. R.; Eising, A. A.; Hünenberger, P. H.; Krüger, P.; Mark, A. E.; Scott, W. R. P.; Tironi, I. G. *Biomolecular Simulations: the GROMOS96 Manual and User Guide*; Verlag der Fachvereine Hochschulverlag AG an der ETH Zürich: Zürich, Switzerland, 1996; pp 1.
- (57) Berendsen, H. J. C.; Grigera, J. R.; Straatsma, T. P. *J. Phys. Chem.* **1987**, *91*, 6269.
- (58) Hess, B.; Bekker, H.; Berendsen, H. J. C.; Fraaije, J. *J. Comput. Chem.* **1997**, *18*, 1463.
- (59) Evdokimov, A.; Gilboa, A. J.; Koetzle, T. F.; Klooster, W. T.; Schultz, A. J.; Mason, S. A.; Albinati, A.; Frolow, F. *Acta Crystallogr., Sect. B: Struct. Sci.* **2001**, *57*, 213.
- (60) Cros, S.; Hervé du Penhoat, C.; Pérez, S.; Imbert, A. *Carbohydr. Res.* **1993**, *248*, 81.
- (61) Gordon, M.; Lowary, T. L.; Hadad, C. M. *J. Org. Chem.* **2000**, *65*, 4954.
- (62) McCarren, P. R.; Gordon, M. T.; Lowary, T. L.; Hadad, C. M. *J. Phys. Chem. A* **2001**, *105*, 5911.
- (63) Case, D. A.; Cheatham, T.; Darden, T.; Gohlke, H.; Luo, R.; Merz, K.; Onufriev, A.; Simmerling, C.; Wang, B.; Woods, R. J. *J. Comput. Chem.* **2005**, *26*, 1668.
- (64) Lindahl, E.; Hess, B.; van der Spoel, D. *J. Mol. Model.* **2001**, *7*, 306.
- (65) Stortz, C. A.; Johnson, G. P.; French, A. D.; Csonka, G. I. *Carbohydr. Res.* **2009**, *344*, 2217.
- (66) Wolfe, S. *Acc. Chem. Res.* **1972**, *5*, 102.
- (67) de Leeuw, H. P. M.; Haasnoot, C.; Altona, C. *Isr. J. Chem.* **1980**, *20*, 108.
- (68) Angyal, S. J. *Aust. J. Chem.* **1968**, *21*, 2737.
- (69) Angyal, S. J. *Angew. Chem., Int. Ed.* **1969**, *8*, 157.
- (70) Angyal, S. J.; Kondo, Y. *Carbohydr. Res.* **1980**, *81*, 35.
- (71) Angyal, S. J.; Pickles, V. A. *Aust. J. Chem.* **1972**, *25*, 1695.
- (72) Džakula, Z.; Westler, W. M.; Edison, A. S.; Markley, J. L. *J. Am. Chem. Soc.* **1992**, *114*, 6195.
- (73) Houseknecht, J.; Lowary, T. L. *J. Org. Chem.* **2002**, *67*, 4150.
- (74) Gandhi, N. S.; Mancera, R. L. *Carbohydr. Res.* **2010**, *345*, 689.
- (75) Schnupf, U.; Willett, J.; Momany, F. *Carbohydr. Res.* **2010**, *345*, 503.
- (76) Allinger, N. L.; Chen, K.; Lii, J.; Durkin, K. A. *J. Comput. Chem.* **2003**, *24*, 1447.
- (77) Lii, J.; Allinger, N. L. *J. Phys. Chem. A* **2008**, *112*, 11903.
- (78) Brisson, J. R.; Uhrinova, S.; Woods, R. J.; van der Zwan, M.; Jarrell, H. C.; Paoletti, L. C.; Kasper, D. L.; Jennings, H. J. *Biochemistry* **1997**, *36*, 3278.
- (79) Corzana, F.; Motawia, M. S.; Hervé du Penhoat, C.; Pérez, S.; Tschampel, S. M.; Woods, R. J.; Engelsens, S. *J. Comput. Chem.* **2004**, *25*, 573.
- (80) Gonzalez-Outeirino, J.; Kadirvelraj, R.; Woods, R. J. *Carbohydr. Res.* **2005**, *340*, 1007.
- (81) Gonzalez-Outeirino, J.; Kirschner, K. N.; Thobhani, S.; Woods, R. J. *Can. J. Chem.* **2006**, *84*, 569.
- (82) Woods, R. J. *Glycoconjugate J.* **1998**, *15*, 209.
- (83) Caldwell, J. W.; Kollman, P. A. *J. Phys. Chem.* **1995**, *99*, 6208.
- (84) Gao, J. L.; Habibollahzadeh, D.; Shao, L. *J. Phys. Chem.* **1995**, *99*, 16460.
- (85) Kaminski, G. A.; Stern, H. A.; Berne, B. J.; Friesner, R. A. *J. Phys. Chem. A* **2004**, *108*, 621.
- (86) Noskov, S. Y.; Lamoureux, G.; Roux, B. *J. Phys. Chem. B* **2005**, *109*, 6705.
- (87) Wang, J. M.; Cieplak, P.; Kollman, P. A. *J. Comput. Chem.* **2000**, *21*, 1049.
- (88) Yu, H.; Geerke, D. P.; Liu, H.; van Gunsteren, W. E. *J. Comput. Chem.* **2006**, *27*, 1494.
- (89) Anisimov, V. M.; Vorobyov, I. V.; Roux, B.; MacKerell, A. D. *J. Chem. Theory Comput.* **2007**, *3*, 1927.
- (90) Vorobyov, I.; Anisimov, V. M.; Greene, S.; Venable, R. M.; Moser, A.; Pastor, R. W.; MacKerell, A. D. *J. Chem. Theory Comput.* **2007**, *3*, 1120.
- (91) Ponder, J. W.; Wu, C.; Ren, P.; Pande, V. S.; Chodera, J. D.; Schnieders, M. J.; Haque, I.; Mobley, D. L.; Lambrecht, D. S.; DiStasio, R. A.; Head-Gordon, M.; Clark, G. N. I.; Johnson, M. E.; Head-Gordon, T. *J. Phys. Chem. B* **2010**, *114*, 2549.

CT100450S